

FoPro-KD: Fourier Prompted Effective Knowledge Distillation for Long-Tailed Medical Image Recognition

Marawan Elbatel^{1,2}, Robert Martí², and Xiaomeng Li¹

¹The Hong Kong University of Science and Technology

²Computer Vision and Robotics Institute, University of Girona

mkfmeibatel@connect.ust.hk, robert.marti@udg.edu,

eexmli@ust.hk

Abstract

Representational transfer from publicly available models is a promising technique for improving medical image classification, especially in long-tailed datasets with rare diseases. However, existing methods often overlook the frequency-dependent behavior of these models, thereby limiting their effectiveness in transferring representations and generalizations to rare diseases. In this paper, we propose FoPro-KD, a novel framework that leverages the power of frequency patterns learned from frozen pre-trained models to enhance their transferability and compression, presenting a few unique insights: 1) We demonstrate that leveraging representations from publicly available pre-trained models can substantially improve performance, specifically for rare classes, even when utilizing representations from a smaller pre-trained model. 2) We observe that pre-trained models exhibit frequency preferences, which we explore using our proposed Fourier Prompt Generator (FPG), allowing us to manipulate specific frequencies in the input image, enhancing the discriminative representational transfer. 3) By amplifying or diminishing these frequencies in the input image, we enable Effective Knowledge Distillation (EKD). EKD facilitates the transfer of knowledge from pre-trained models to smaller models. Through extensive experiments in long-tailed gastrointestinal image recognition and skin lesion classification, where rare diseases are prevalent, our FoPro-KD framework outperforms existing methods, enabling more accessible medical models for rare disease classification.

1 Introduction

Convolutional neural networks (CNNs) have shown remarkable performance in medical image classification.

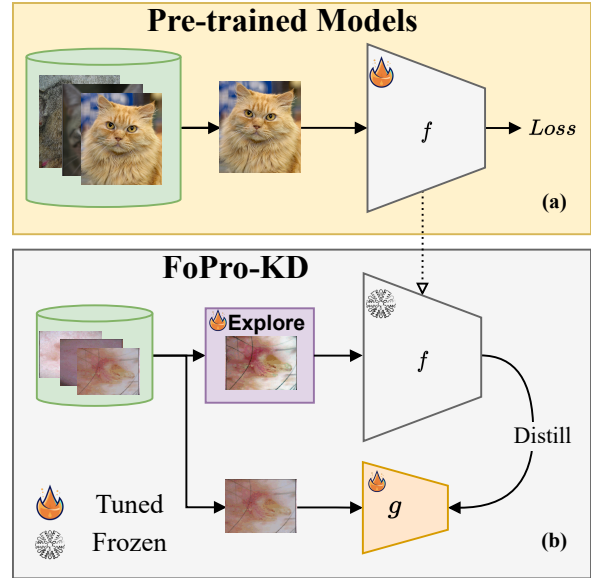


Figure 1: (a) The pre-trained model “free lunch” assumes specific frequency patterns in input data. (b) Our FoPro-KD approach explicitly queries the model to identify meaningful frequency patterns for distillation.

However, the scarcity of labeled medical image datasets can limit their applicability, particularly in datasets with long-tailed distributions where rare classes are present. Transfer learning has emerged as a promising approach to tackle this challenge by fine-tuning pre-trained models on natural images to medical image datasets. Nevertheless, a crucial issue in transfer learning is to devise an efficient technique that preserves the generalization capabilities of large pre-trained models while remaining compact enough for practical deployment in a clinical environment.

Publicly available pre-trained models, such as CLIP [27], MoCo [15], and BYOL [14], have attracted

considerable attention in the medical imaging community due to their promising generalization capabilities as “free lunch” models [9]. However, the extensive model complexity and significant computational resource requirements associated with these pre-trained models can limit their applicability in clinical settings in low infrastructure, point-of-care testing, and edge devices. Moreover, fine-tuning these models on smaller, long-tailed medical image datasets offer reduced performance on the tail classes / rare diseases compared to linear probing; see comparisons in Table 7. Therefore, it is highly demanded to develop an effective transfer learning approach to leverage the generalization capabilities of large pre-trained models while maintaining performance for tail classes in the target datasets.

Recently, Yu *et al.* [35] quantified the frequency bias in neural networks and proposed a method for guiding the network to tune its frequency by utilizing a Sobolev norm that expands the L2 norm. Although their approach was limited to Neural Tangent Kernels (NTK) and focused on quantifying the frequency bias on a broad frequency basis without investigating the specific frequency patterns captured by pre-trained networks, their work inspired us to explore and exploit these patterns from publicly available pre-trained models, known as “free lunch models”, conditioned on a target medical dataset to improve the representation learning for rare disease classification. Pre-trained models, known as “free lunch models” encode frequency patterns through their convolutional and pooling operations during pre-training. Each filter in the convolutional layer acts as a frequency filter, capturing distinct patterns in the input data, while pooling operations further amplify or attenuate these patterns. This frequency-dependent behavior can introduce biases in the model, making it more sensitive to certain frequency patterns and less sensitive to others, which may not align with the frequency characteristics of target medical data.

To address this issue, we explore these frequency patterns and manipulate the input data to highlight or diminish them, optimizing the transfer of representations from the pre-trained model on natural images to a smaller target model, as illustrated in Figure 1. This allows us to enhance the performance of the target model in long-tailed medical applications, including gastrointestinal image recognition and skin lesion classification.

To this end, we propose FoPro-KD (Fourier-prompted Effective Knowledge Distillation) to enhance the transferability of publicly available pre-trained models from natural imaging to long-tailed medical image classification tasks. FoPro-KD consists of two stages: exploration and exploitation. In the exploration stage, a Fourier prompt generator (FPG) is trained to unleash the frequency patterns based on the frozen pre-trained model, conditioned on the target medical domain, for effective representational transfer. In the

exploitation stage, the FPG generates targeted perturbation as Fourier amplitude spectral prompts for effective knowledge distillation (EKD). EKD compresses the generalization capabilities of “free lunch models” into smaller medical imaging models more efficiently, enhancing tail classes / rare diseases recognition. Additionally, adversarial knowledge distillation (AKD) facilitates the exploration and exploitation process by iteratively learning the FPG, thereby promoting diverse patterns and avoiding mode collapse.

Our proposed method represents a novel approach in the field of medical imaging in generating targeted perturbation to pre-trained models on natural images. Rather than synthesizing worst-case images as in the literature of adversarial domain adaptation, we utilize a source-free frozen pre-trained model trained on natural images to learn Fourier spectrum amplitudes that are necessary for exploring these free lunch models. By exploring the frequency patterns learned by the pre-trained model, which we find to be efficient in exploiting its generalization capabilities, we can leverage free lunch models’ generalization capabilities for a target medical imaging dataset without fine-tuning these models on the target dataset.

The main contributions of this work can be summarized as the following:

- We demonstrate that effective knowledge distillation (EKD) from frozen pre-trained models on natural images to a target smaller medical imaging model can be just as effective as traditional long-tailed methods, thanks to their generalization capabilities.
- We show that our generated Fourier prompts are highly effective in generating targeted perturbations that can further improve the generalization capabilities of our proposed EKD, particularly in long-tailed medical image classification tasks.
- We introduce a novel framework called FoPro-KD, which achieves state-of-the-art performance on two long-tailed medical image classification benchmarks, demonstrating the effectiveness of our method in improving the transferability of pre-trained models to medical imaging tasks.

2 Related Work

In this section, we provide a review of the literature related to transfer learning with prompt tuning, adversarial domain adaptation, and long-tailed learning methods. We highlight the relevant works in these areas and discuss their contributions.

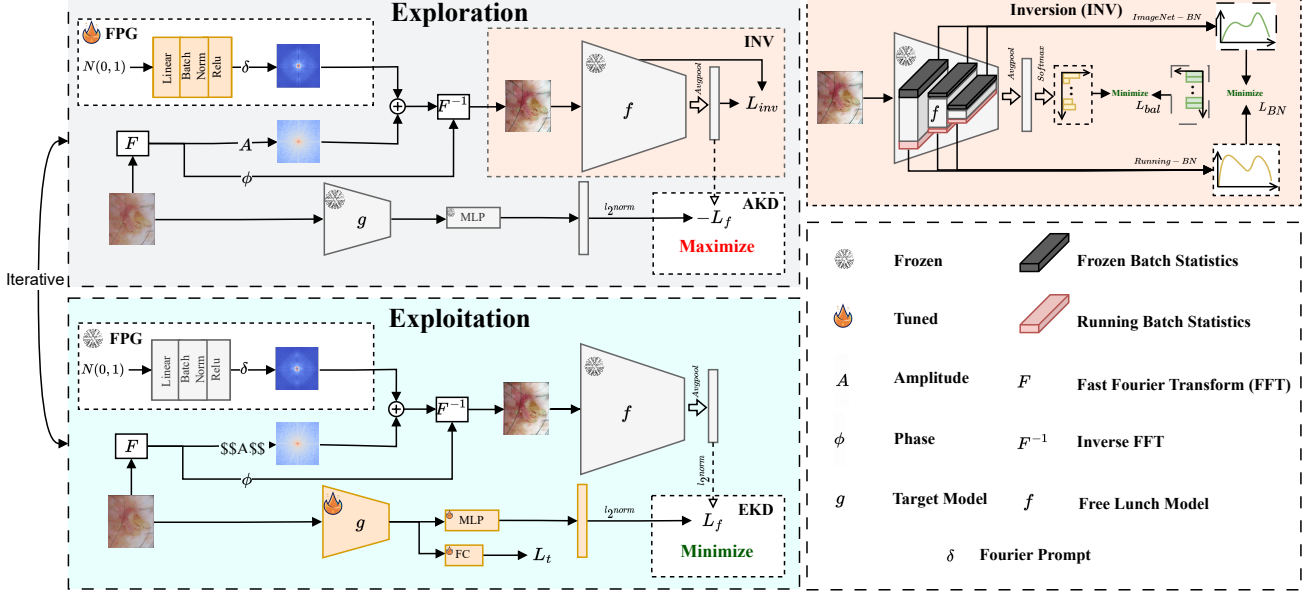


Figure 2: Our proposed FoPro-KD framework has two phases: exploration and exploitation. In the exploration phase, the FPG generates Fourier prompts to capture frequency patterns of the frozen pre-trained model f . In the exploitation phase, the proposed effective knowledge distillation (EKD) module distills the knowledge from f into the target model g , guided by the Fourier prompt generator (FPG). Our framework can iteratively alternate between the exploration and exploitation phases using adversarial knowledge distillation (AKD) to enhance representation distillation and learning efficiency of g .

2.1 Transfer Learning

In recent years, transfer learning and fine-tuning have been extensively studied in the literature, with a focus on adapting the feature extractor to fit the target task. However, such approaches can deviate from pre-trained features, resulting in a trade-off between the performance of the majority class (in-distribution or IID) and the rare class (out-of-distribution or OOD). To mitigate similar tradeoffs on IID and OOD datasets, Kumar *et al.* [23] proposed a simple variant of initializing the head with a linear probed version followed by full fine-tuning. Nevertheless, these methods can suffer from deviating semantics and extreme overfitting on long-tailed problems when fully fine-tuning large pre-trained models. Prompt tuning arises in vision to address these issues for efficiently fine-tuning large models in vision tasks, similar to natural language processing (NLP). Jia *et al.* [19] proposed Vision Prompt Transformer (VPT), which adds prompts to vision transformers and exploits the transformer’s location-invariant features for effective fine-tuning. Similar to NLP prompt tuning, Dong *et al.* [10] explored the use of prompt learning for the effective transfer of pre-trained vision transformers for long-tail natural image classification. These methods are specially tailored to vision transforms similar to NLP, failing to find an efficient prompt for transforming the knowledge of CNN vision-pre-trained models, which are important for medical imaging

classification. Recently, Bai *et al.* [1] found that a CNN teacher can benefit vision transformers to fit high-frequency components and proposed HAT to adversarially augment images’ high-frequency components towards improving vision transformers generalization capabilities. Prompt tuning for CNN models can be related to the literature on adversarial learning and domain adaptation.

2.2 Adversarial learning

Adversarial learning has emerged as a popular approach for domain adaptation (DA) and domain generalization (DG). To achieve DA, Huang *et al.* [18] proposed a method that generates adversarial examples from the source dataset and fine-tunes the model on the target dataset using both adversarial and clean examples. Similarly, Kim *et al.* [22] modeled DG as DA to adversarially generate worst-case targets from the source dataset. Chen *et al.* [4] proposed MaxStyle as an adversarial realistic data augmentation utilizing an auxiliary image decoder for robust medical image segmentation. For source-free unsupervised domain adaptation (SFUDA), Hu *et al.* [17] proposed to learn a domain-aware prompt adversarially for a UNet-based model. More recently, Wang *et al.* [32], inspired by Fourier style mining [33], proposed to learn a low-frequency Fourier visual prompt for SFUDA that excelled in segmentation performance. However, all these methods are restricted to source

and target datasets trained for the same closed-set task and often rely on increasing noise to synthesize adversarial examples in DG or on bridging the gap between datasets in DA. Their approaches do not explicitly leverage the frequency patterns captured by pre-trained models on natural images during their pre-training stage, which can aid in representational learning, especially for long-tailed datasets

2.3 Long-Tail Learning

Long-tailed distributions, characterized by severe class imbalance where minority classes are significantly outnumbered by majority classes, are common in many medical imaging tasks, such as skin-lesion classification and gastrointestinal image recognition [2, 6, 31]. Such class imbalance poses challenges for training accurate models, and various approaches have been proposed to address this issue, including data augmentation techniques, re-sampling and re-weighting schemes, and curriculum-based methods. Data augmentation techniques aim to regularize the model by incorporating regularization techniques to enhance the model’s representations. For example, Zhang *et al.* [36] proposed MixUp offering information augmentation to regularize training. However, such regularization needs to be coupled with a balancing scheme to account for the huge class imbalance. Galdran *et al.* [12] proposed Balanced-Mixup, a simple variant of MixUp using class conditional sampling that has compelling capabilities for highly imbalanced medical image classification. Moreover, data augmentation methods usually need to be coupled with different loss re-weighting strategies to account for the label distribution shift that can arise over the test set. Class balancing loss (CB) [7], Label distribution margin (LDAM) [3], and balanced-softmax (BSM) [29] was proposed as modified re-weighting strategies for training models for long-tailed learning. However, these methods often have limitations, such as not effectively addressing the extreme bias from head classes. To address such bias, Kang *et al.* [21] found that the classifier is the major bottleneck for the head classes bias in long-tail learning and proposed a two-stage learning approach that decouples the feature extractor representations from the classifier through a plug-in classifier re-training (cRT). Although cRT increased the performance of multiple long-tailed methods, it did not solve the intra-class imbalance that can restrict the representation extraction [39]. To address the intra-class imbalance, Tang *et al.* [30] proposed invariant feature learning (IFL) through dual environment learning and re-sampling techniques. On the other hand, methods based on curriculum learning, requiring a pre-training stage on the target dataset to extract meaningful representation followed by utilizing these representations, have achieved state-of-the-art performance for long-tailed learning. For example, Zhang *et al.* [37]

achieved SOTA in multiple long-tailed datasets by a two-stage framework. First, by pre-training a teacher model on the target dataset to capture the target dataset representations, followed by a balanced knowledge distillation (BKD) to guide a student model. However, all the aforementioned methods have not utilized the generalization capabilities of publicly available pre-trained models known for their generalizable representations, as they focus more on the problem on a narrow knowledge extraction basis from the target dataset, whereas pre-training and the knowledge gained from natural images have achieved compelling performance in medical imaging as “free lunch models” [9].

In our work, we re-visit long-tailed learning in medical imaging from a free lunch perspective. We demonstrate that the generalizable features from publicly available pre-trained models on natural images can be comparable to different long-tail methods without additional pre-training or fine-tuning of these free lunch models. In addition, we find that these free lunch models have a preferred frequency basis (i.e. styles) for their input that can restrict their distillation in many tasks. To address such preferred styles, we propose to explore these preferred styles through effective prompting on a frequency basis. By exploring the pre-trained models’ frequency patterns and iteratively distilling such knowledge, we can recycle and compress these pre-trained models with no additional training to the target medical task, our approach can be easily utilized with different long-tailed learning schemes as a free lunch distillation, achieving SOTA on multiple long-tailed medical imaging datasets.

3 Method

Figure 2 shows the framework for our proposed FoPro-KD. The training of FoPro-KD consists of two stages: an exploration stage and an exploitation stage. In the exploration stage, we train one linear layer as a Fourier Prompt Generator (FPG) to generate Fourier amplitude spectral prompts, δ , conditional on our target medical data, allowing us to explore the representations of the free lunch model, f , by explicitly asking what frequency patterns on the input lead to meaningful representations. This is done while freezing f , pre-trained on natural imaging dataset (ex: MoCov2 on ImageNet [15]). In the exploitation stage, we effectively distill these generalizable representations to a smaller target medical imaging model, g through our proposed Effective Knowledge Distillation (EKD). To make the Fourier prompts more diverse while being representative of f , we perform multiple iterations of the exploration and exploitation stages by an Adversarial Knowledge Distillation (AKD). This allows us to effectively exploit the generalization capabilities of large pre-trained models and compress them into smaller student networks that are useful for

practical medical imaging deployment in a clinical setting. Our framework provides a scalable and efficient approach to distilling knowledge from pre-trained models, with potential applications in various medical imaging tasks.

3.1 Fourier Prompt Generation

To attain optimal representational transfer, publicly available pre-trained models necessitate input data that closely align with their preferences. In this regard, training a conditional generative adversarial network (CGAN) [26] to guide the target dataset towards these preferences can substantially modify the semantics of the dataset. As shown in Figure 3, training a CGAN with deep inversion causes modification in the semantics of the target dataset in the highly informative regions conditional on the semantics of the pre-training dataset, ImageNet [8].

Recent research by Yu *et al.* [35] has shown theoretically that neural networks can be sensitive to certain frequencies without explicitly considering the frequency patterns captured during pre-training deep neural networks (DNNs). Therefore, we aim to explore this frequency-dependent behavior of CNNs and enable frozen pre-trained models to output representations through prompting on a frequency basis, which is facilitated by our proposed Fourier Prompt Generator (FPG).

FPG employs a random noise vector, z , to generate a three-dimensional Fourier amplitude prompts, $\delta = FPG(z)$, one for each channel respectively, enabling the modification of the target dataset by emphasizing or suppressing specific frequency patterns preferred and captured by “free lunch models” on the source natural images dataset. Although these preferred patterns relied on the deep learning dynamics of the “free lunch models”, the FPG can be trained to unleash such patterns and generate Fourier prompts that are the preference of the “free lunch model” conditioned on our target medical dataset. This feature plays a critical role in effective knowledge distillation.

Let the Fourier decomposition of an image x be $F(x)$, which consists of the amplitude A and phase ϕ components:

$$F(x) = A \odot e^{i\phi} \quad (1)$$

To interpolate the Fourier amplitude between the input image and the generated Fourier prompt, we use a mixing coefficient, denoted by α and sampled uniformly from 0 to 1, resulting in a new Fourier amplitude spectrum \hat{A} :

$$\hat{A}_{ij} = \alpha A_{ij} + (1 - \alpha) \delta_{ij} \quad (2)$$

where A_{ij} represents the Fourier amplitude of the input image, δ_{ij} represents the the generated Fourier prompt, and ij are the indices of the Fourier coefficients.

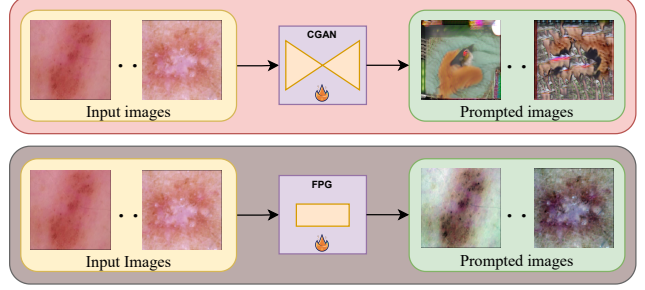


Figure 3: Using a conditional GAN (CGAN) to manipulate the input dataset changes the image semantics in highly informative regions compared to surpassing or amplifying certain frequencies in these regions with FPG.

The modified Fourier coefficients are then transformed back using the inverse Fourier transform to generate the modified image, denoted by \hat{x} ,

$$\hat{x} = F^{-1}(\hat{A} \odot e^{i\phi}) \quad (3)$$

where F^{-1} denotes the inverse Fourier transform.

We train the Fourier prompt generator in the exploration phase while freezing all other modules. Specifically, we feed \hat{x} to the frozen pre-trained feature extractor, f , and utilize the batch regularization technique that was first introduced in [34]. This technique minimizes the divergence between the feature statistics, which include the mean and variance of the features, and the corresponding batch normalization statistics by assuming a Gaussian distribution:

$$\mathcal{L}_{BN}(x) = \sum_{l \in f} D\left(N\left(\mu_l(\hat{x}), \sigma_l^2(\hat{x})\right) \middle| N\left(\mu_l, \sigma_l^2\right)\right), \quad (4)$$

where D is the L2 divergence loss, $N(\mu_l(\hat{x}), \sigma_l^2(\hat{x}))$ is the feature statistics of the modified input batch \hat{x} , $N(\mu_l, \sigma_l^2)$ is the batch normalization statistics of the frozen model, f , and l indexes the layers of f .

To better capture the frozen pre-trained model’s learned frequency patterns and avoid skewing in the learning of the Fourier Prompt Generator (FPG), we propose a regularization approach that encourages the synthesis of Fourier prompts with a more balanced distribution of activations across the final pre-classification features. This is achieved by maximizing the entropy of the free lunch model output towards a uniform distribution where each feature has an equal probability of being activated as

$$\mathcal{L}_{bal} = \sum_{i=1}^C p_i \log p_i \quad (5)$$

where C is the dimension of the final pre-classification features, and p_i is the i -th element of the softmax output p of the frozen pre-trained model on the target modified

data \hat{x} . This approach avoids bias towards any particular feature and promotes the generalization ability of the learned Fourier prompts.

The final inversion loss \mathcal{L}_{inv} to train the FPG module is defined as the combination of the batch normalization loss, \mathcal{L}_{BN} , and the balancing loss, \mathcal{L}_{bal} , as

$$\mathcal{L}_{inv} = \mathcal{L}_{BN} + \mu \mathcal{L}_{bal} \quad (6)$$

where μ is the weighting factor for the balancing regularization.

By combining this balanced regularization term with the batch statistics losses, the generated Fourier prompts can exhibit higher entropy while being specific to the frozen pre-trained model’s desired frequencies to better benefit the knowledge distillation. To ensure that the FPG-generated Fourier prompts produce valid Fourier amplitudes, we apply a Hermitian constraint.

The exploration phase ensures that the Fourier generator produces styles that are consistent with the preferred frequency patterns of the free lunch model while also avoiding overfitting specific styles.

Our training approach for the FPG can be seen as a deep inversion method in the literature of data-free knowledge distillation [11]. However, our method is unique in the learnable and target objectives, in addition, conditioned on a cross-task target dataset, which makes it more challenging.

3.2 Exploitation with Effective Knowledge Distillation

Large pre-trained models available to the public possess remarkable generalization capabilities that can assist in the classification of rare diseases. It has been observed that performing linear probing on these models yields high-accuracy results on out-of-distribution (OOD) datasets. However, complete fine-tuning of these models may lead to distortion of these highly generalizable representations [23]. To this end, we propose Effective Knowledge Distillation (EKD), which aims to compress the generalization capabilities of the free lunch models while maintaining generalizable performance on the target data using a smaller model.

To achieve this, we utilize a small target model with a feature extractor $g(\cdot)$ to be trained on the target medical dataset, along with a large frozen publicly available pre-trained encoder $f(\cdot)$ (free lunch model). To compare the latent features of the target model with those of the free lunch model, we add a 2-layer MLP on top of the smaller target feature extractor, $g(\cdot)$.

To generate the necessary encodings for distillation, we sample an image x uniformly from the target dataset \mathcal{D} and use prompt mixing following Equation (3) to obtain \hat{x} ,

while freezing FPG. This allows us to navigate the representation of f based on the styles and frequencies it was trained on.

From here, we generate two encodings: a *projection* $y = MLP(g(x))$ and a *target representation* $t = f(\hat{x})$ from our target network and the large frozen pre-trained network, respectively. We then L2-normalize both encodings and distill the information from the large pre-trained model to the smaller target model using a mean squared error loss as our distillation loss between both encodings, as

$$\mathcal{L}_f = 2 - 2 \cdot \langle y, t \rangle. \quad (7)$$

While previous approaches [5] aims to reduce the performance gap between the teacher and student models on the same task, our proposed distillation loss is designed to narrow the generalization capabilities of free lunch models to a different task, which our student model is being trained on. This approach can act as an implicit regularization technique, leveraging the discriminative generalization capabilities of large pre-trained model features for the tail classes. Specifically, our approach encourages the $g(\cdot)$ to generalize well to the tail classes of the target task, which may be rare and difficult to identify without additional guidance. We denote the exploitation loss, $\mathcal{L}_{exploit}$, to minimize at each training step as:

$$\mathcal{L}_{exploit} = \mathcal{L}_t + \lambda_f \mathcal{L}_f, \quad (8)$$

where \mathcal{L}_t is a target loss for long-tail learning [29].

3.3 Exploration with Adversarial Distillation

To ensure that the learned Fourier amplitudes become more diverse while being representative of the natural image styles, thus alleviating any representational mode collapse issue in distillation, we propose to further enhance the Fourier prompt generation by navigating the latent space of the free lunch model with an iterative adversarial loss.

To achieve this, we propose maximizing the proposed effective knowledge distillation (EKD) loss between the free lunch model and the target model for iterative exploration. The final exploration loss, $\mathcal{L}_{explore}$, to be optimized is given by:

$$\mathcal{L}_{explore} = -\gamma \lambda_f \mathcal{L}_f + \mathcal{L}_{inv} \quad (9)$$

Here we maximize the similarity between the free-lunch model and the target model, as described in Equation (7). This adversarial loss is weighted by a hyperparameter γ , which determines the strength of the adversarial training. Unlike standard adversarial training, we aim to explore the free-lunch model, so we set γ between 0 and 1, with an upper bound of the exploitation distillation factor λ_f . This is similar to the training of generative adversarial networks

(GANs) [13]. To this end, we choose a value of $\gamma = 0.3$ and provide an ablation study to validate our choice. \mathcal{L}_{inv} ensures that the prompts generated by the Fourier prompt generator accurately represent the pre-trained model.

4 Experiments

4.1 Datasets

ISIC-LT is a challenging long-tailed skin lesion classification dermatology dataset from ISIC [6]. The dataset consists of eight classes and we create a long-tailed version of it following [20] using a Pareto distribution sampling approach. To ensure class imbalance and rare disease diagnosis, we set the class imbalance ratio to be 100, 200, 500 and select 50 and 100 images from each class for the validation and test sets respectively, from the remaining samples. We assess the model performance on the held-out test set. Results for each method are averaged over 5 runs, each with a different sampled train, validation, and held-out test set. To assess the model performance on the balanced test set, we follow previous guides [28] to report the Mathew-correlation coefficient (“MCC”), accuracy (“Acc”), and f1-score.

Hyperkvasir is a long-tailed dataset of 10,662 gastrointestinal tract images, consisting of 23 classes representing different anatomical and pathological landmarks and findings. To analyze the long-tailed distribution, we categorize the 23 classes into three groups: Head (with over 700 images per class), Medium (with 70 to 700 images per class), and Tail (with fewer than 70 images per class) based on their class counts. Notably, the Tail class includes a distinct class for Barrett’s esophagus, which presents as short segments and is considered a premalignant condition that may progress to cancer. Additionally, the Tail classes encompass two transitional grades of ulcerative colitis, an inflammatory bowel disease, and the terminal ileum, which confirms a complete colonoscopy but cannot be differentiated endoscopically from parts of the small bowel. Since the official test set only contains 12 classes, we follow the evaluation approach of BalMixUp [12] and assess our model’s performance using a stratified 5-fold cross-validation method. To assess the performance with a high imbalance test set, We report the balanced accuracy “B-Acc” that considers the average per class accuracy and denote the performance of the few-shot division (“Head”, “Medium”, “Tail”) and their average results denoted as “All”.

4.2 Implementation Details

For both datasets, we use checkpoints pre-trained on MoCo-RN50 [15] available online as the free lunch models

trained on ImageNet for compressing its generalization capabilities unless otherwise stated. We use Adam optimizer with a learning rate of $3e-4$ for all methods on the ISIC-LT dataset. On the other hand, we follow [12] for the HyperKvasir dataset and use SGD with a cosine annealing scheduler [24] with a maximum learning rate of 0.01. For both datasets and all methods, we use a ResNet-18 as the target model with a batch size of 32 and apply augmentations techniques such as random crop and flipping. Images are resized to 224x224, and we train all methods until there is no further increase in the validation set for 20 epochs with a total of 100 epochs. To ensure a fair comparison between different methods, we keep all hyperparameters the same. We set λ_f to 3, μ to 10, and γ to 0.3 on both datasets. For every 5 training epochs exploited, we explore the pre-trained model for one epoch to balance the training process.

4.3 Baselines

Our experimental evaluation compares the performance of our proposed FoPro-KD method against several state-of-the-art long-tailed learning approaches. Specifically, we evaluate (1) re-sampling (RS) and re-weighting (RW) techniques, (2) various data augmentation techniques including MixUp [36], and its balanced version (BalMixUp) [12], specifically designed for medical image classification (3) Modified Loss re-weighting schemes including Class balancing (CB) loss [7], and label-distribution-aware margin (LDAM) loss with curriculum delayed reweighting (DRW) [3], and the balanced softmax (BSM) [29] (4) A recent curriculum-based method, balanced Knowledge Distillation (BKD) [37].

4.4 Performance on ISIC-LT

We present the performance of our proposed FoPro-KD approach for long-tailed skin lesion classification on the ISIC-LT dataset in Table 1. Our approach outperforms all baselines across all class imbalance ratios and evaluation metrics, demonstrating its effectiveness. FoPro-KD improves the performance of the naive cross entropy by 10.7%, 12.4%, and 12.4% on the “MCC” over the balanced test set for class imbalance ratios of 1:100, 1:200, and 1:500, respectively. Compared to the baseline, BSM [29], FoPro-KD improves the “MCC” being sensitive for class imbalance by 4.5%, 5.6%, and 3.7% for imbalance ratios of 1:100, 1:200, and 1:500, respectively. Furthermore, it increases the performance of the baseline, BSM [29], by 3.7%, 4.7%, and 2.9% on the “Acc” metric for class imbalance ratios of 1:100, 1:200, and 1:500, respectively. Compared to the best-performing baseline on imbalance ratios 1:200 and 1:500, BKD [37], our method outperforms it by 6.0%, 3.0%, and 3.0% on the “MCC” for the three im-

Table 1: Experimental results on long-tailed skin lesion classification (ISIC-LT) are presented, considering different class imbalance ratios. The methods used include naive cross-entropy (CE), class sampling (RS), and loss re-weighting (RW). The reported results are averaged over 5 runs on a balanced held-out test set.

Method	Class Imbalance Ratio								
	1:100			1:200			1:500		
	MCC	Acc	F1-Score	MCC	Acc	F1-Score	MCC	Acc	F1-Score
CE	57.64 (± 1.6)	62.15 (± 1.4)	65.52 (± 1.4)	53.71 (± 1.7)	58.33 (± 1.5)	62.72 (± 1.2)	44.9 (± 2.2)	50.22 (± 1.9)	55.83 (± 2.0)
RS	59.46 (± 1.0)	63.9 (± 0.9)	67.04 (± 0.6)	55.53 (± 1.6)	60.35 (± 1.5)	63.71 (± 1.4)	48.54 (± 1.4)	53.73 (± 1.2)	59.15 (± 1.1)
RW	56.03 (± 2.3)	61.2 (± 1.9)	63.17 (± 2.2)	52.22 (± 1.6)	57.95 (± 1.4)	59.48 (± 1.5)	46.77 (± 0.4)	52.8 (± 0.4)	55.36 (± 0.7)
EKD (ours)	61.37 (± 1.8)	65.42 (± 1.6)	68.49 (± 1.5)	57.57 (± 1.1)	61.9 (± 0.9)	65.41 (± 1.2)	49.16 (± 1.9)	54.2 (± 1.8)	59.24 (± 1.4)
CB [7]	57.28 (± 2.3)	62.23 (± 2.1)	64.36 (± 1.6)	53.58 (± 2.1)	58.9 (± 2.1)	61.27 (± 1.6)	47.16 (± 1.2)	53.17 (± 1.1)	55.9 (± 1.6)
LDAM-DRW [3]	60.27 (± 0.7)	64.88 (± 0.6)	66.17 (± 0.7)	55.85 (± 1.6)	60.98 (± 1.5)	62.25 (± 1.3)	50.34 (± 1.1)	55.98 (± 0.8)	57.95 (± 1.3)
BSM [29]	63.88 (± 1.9)	68.15 (± 1.7)	69.25 (± 1.6)	60.47 (± 1.6)	65.12 (± 1.4)	66.2 (± 1.2)	53.61 (± 1.1)	59.02 (± 1.0)	60.27 (± 0.9)
MixUp [36]	55.53 (± 1.8)	59.91 (± 1.9)	64.33 (± 1.0)	48.96 (± 2.1)	53.59 (± 2.2)	59.68 (± 1.5)	43.03 (± 1.6)	48.12 (± 1.5)	54.36 (± 1.1)
BalMixup [12]	61.35 (± 1.8)	65.5 (± 1.5)	68.46 (± 1.5)	56.36 (± 3.9)	61.0 (± 3.5)	64.37 (± 3.5)	50.26 (± 1.1)	55.3 (± 1.1)	60.29 (± 0.7)
BKD [37]	62.24 (± 1.6)	66.55 (± 1.6)	68.35 (± 0.9)	<u>63.06 (± 1.4)</u>	<u>67.42 (± 1.2)</u>	<u>68.32 (± 1.3)</u>	<u>54.25 (± 1.3)</u>	<u>59.59 (± 1.1)</u>	<u>60.5 (± 1.2)</u>
FoPro-KD (ours)	68.33 (± 2.3)	71.8 (± 2.0)	73.88 (± 1.9)	66.08 (± 1.5)	69.8 (± 1.3)	71.91 (± 1.2)	57.33 (± 1.5)	61.9 (± 1.5)	64.43 (± 1.3)

Table 2: Experimental results on long-tailed Gastrointestinal image recognition. The top-1 accuracy is reported using a shot-based division (“Head”, “Medium”, “Tail”) to address test set imbalance, and their average “All”, along with the resilient metric “B-Acc” for class imbalance.

Method	Metrics				
	Head	Medium	Tail	All	B-Acc
CE	93.14 (± 0.7)	74.7 (± 1.2)	4.05 (± 4.8)	57.3 (± 1.3)	58.81 (± 1.1)
RS	88.89 (± 3.9)	72.37 (± 3.2)	11.38 (± 10.4)	57.55 (± 1.8)	58.84 (± 1.6)
RW	87.43 (± 1.8)	70.04 (± 2.5)	20.28 (± 7.6)	59.25 (± 2.0)	60.19 (± 1.8)
CB [7]	88.22 (± 1.5)	70.36 (± 1.7)	18.04 (± 9.8)	58.88 (± 2.7)	59.88 (± 2.5)
LDAM-DRW [3]	92.53 (± 0.6)	69.4 (± 1.5)	24.55 (± 9.1)	62.16 (± 2.5)	62.79 (± 2.2)
BSM [29]	91.4 (± 0.7)	65.96 (± 3.0)	26.54 (± 7.7)	61.3 (± 1.9)	61.7 (± 1.6)
MixUp [36]	94.23 (± 0.6)	75.08 (± 1.2)	3.93 (± 3.3)	57.75 (± 1.0)	59.25 (± 0.9)
BalMixup [12]	92.16 (± 1.1)	74.57 (± 1.7)	8.44 (± 3.8)	58.39 (± 1.1)	59.8 (± 0.9)
BKD [37]	92.53 (± 0.9)	69.88 (± 5.0)	17.43 (± 12.6)	59.95 (± 2.7)	60.81 (± 2.3)
FoPro-KD (ours)	92.78 (± 2.0)	68.08 (± 6.5)	31.9 (± 8.5)	64.25 (± 0.8)	64.59 (± 0.9)

balance ratios, respectively. Notably, our approach outperforms BKD on the f1-score with 3.6% and 3.9% performance gains over the imbalance ratios 1:200 and 1:500 without additional pre-training on the target dataset.

It is worth mentioning that our proposed EKD used with the naive cross-entropy loss improves performance by 3.7%, 3.9%, and 4.3% on the “MCC” metric for class imbalance ratios of 1:100, 1:200, and 1:500, respectively, without the need for FPG or special loss re-weighting or re-sampling, demonstrating the need to leverage the free lunch models for the long-tail problems in an effective way.

4.5 Performance on HyperKvasir

We present the experimental results of our long-tailed gastrointestinal image recognition approach in Table 2. Our approach outperformed the naive cross-entropy method by 7.0% and 5.8% for the imbalance test-set and increased the performance of the baseline [29] by 2.9% and 2.9% on the “All” and “B-Acc” metrics respectively. Moreover, our method achieved the highest performance for the “Tail” (31.9%), highlighting its ability to capture rare diseases.

Our method also outperformed the state-of-the-art BKD [37] on the HyperKvasir dataset. BKD relies on distilling a pre-trained teacher model over the target dataset, which can amplify bias over the head classes if the teacher model failed to capture the tail classes. In contrast, our approach leverages the discriminative generalizable features of free lunch models to achieve superior performance. Specifically, our approach outperformed BKD by 4.3% and 3.8% over “All” and “B-Acc”, respectively.

4.6 Ablation Studies

Effectiveness of EKD and FPG In Table 3, we present an ablation study of our proposed components over the ISIC-LT. Our approach combines a Fourier prompt generator (FPG) with effective knowledge distillation (EKD) to exploit the pre-trained model. Our experimental results on the ISIC-2019 dataset demonstrate that EKD alone improves performance by 1.5%, 3.6%, and 2.2% on the “MCC” for the three imbalance ratios, respectively. By adding FPG, we achieve even higher performance gains of 4.5%, 5.6%, and 3.7% on the “MCC” for class imbalance ratios of 1:100, 1:200, and 1:500 compared to the baseline, BSM [29].

Table 3: Ablation of FLKD and FPG on three imbalance ratios on ISIC-LT

	EKD	FPG	Metric		
			MCC	Acc	F1-Score
			ISIC-LT (1:100)		
BSM [29]	×	×	63.88 (± 1.9)	68.15 (± 1.7)	69.25 (± 1.6)
w/ EKD (ours)	✓	×	65.36 (± 3.3)	69.47 (± 2.9)	70.42 (± 2.9)
FoPro-KD (Ours)	✓	✓	68.33 (± 2.3)	71.8 (± 2.0)	73.88 (± 1.9)
ISIC-LT (1:200)					
BSM [29]	×	×	60.47 (± 1.6)	65.12 (± 1.4)	66.2 (± 1.2)
w/ EKD (ours)	✓	×	64.08 (± 1.4)	68.35 (± 1.2)	69.19 (± 1.3)
FoPro-KD (Ours)	✓	✓	66.08 (± 1.5)	69.8 (± 1.3)	71.91 (± 1.2)
ISIC-LT (1:500)					
BSM [29]	×	×	53.61 (± 1.1)	59.02 (± 1.0)	60.27 (± 0.9)
w/ EKD (ours)	✓	×	55.81 (± 1.6)	60.92 (± 1.4)	62.02 (± 1.3)
FoPro-KD (Ours)	✓	✓	57.33 (± 1.5)	61.9 (± 1.5)	64.43 (± 1.3)

Our proposed EKD and FPG methods provide complementary benefits for improving the performance of the target model in the long-tailed setting. While FPG helps to explore the pre-trained model’s latent space by explicitly asking what frequency patterns it wants in the input, EKD helps to exploit the pre-trained model’s generalizable representation. By leveraging pre-trained models’ frequency patterns, our approach achieves the best performance on the ISIC-LT dataset and HyperKvasir dataset, highlighting the importance of utilizing pre-trained models for medical image classification with long-tailed class distributions.

Ablation of Free Factor We present an ablation study of the weighting factor, λ_f , for the exploitation proposed in Equation (8), with experiments conducted on the ISIC-LT imbalance factor 1:500 without our proposed FPG. The results are summarized in Table 4.

Table 4: Exploitation λ_f ablation without FPG on the ISIC-LT (Acc)

Method	ISIC-LT (1:500)			
	$\lambda_f = 0$	$\lambda_f = 1$	$\lambda_f = 3$	$\lambda_f = 5$
EKD	59.02 (± 1.0)	59.52 (± 2.4)	60.92 (± 1.4)	60.47 (± 1.6)

We find that using effective knowledge distillation (EKD) with a factor of $\lambda_f = 3$ improves the performance on the ISIC-LT dataset compared to the baseline ($\lambda_f = 0$), [29], achieving an “Acc” gain of 1.9%. However, a higher value of λ_f can deviate from the learning objective.

Table 5: Ablation of Exploration on the ISIC-LT 1:500 dataset

	\mathcal{L}_{inv}	\mathcal{L}_{adv}	Metric		
			MCC	Acc	F1
EKD (ours)	×	×	55.81 (± 1.6)	60.92 (± 1.4)	62.02 (± 1.3)
Explore only	✓	×	56.80 (± 1.4)	61.59 (± 1.2)	63.73 (± 1.8)
FoPro-KD	✓	✓	57.33 (± 1.5)	61.9 (± 1.5)	64.43 (± 1.3)

Effectiveness of FPG To evaluate the importance of \mathcal{L}_{inv} , we perform an ablation study and report our results in Table 5. We find that learning the FPG and exploring the frozen pre-trained model with only \mathcal{L}_{inv} leads to an improvement over our proposed EKD with an increase of 1.0 % and 1.7% on “MCC” and f1-score, respectively. Moreover, when using iterative adversarial knowledge distillation (AKD) along with \mathcal{L}_{inv} , we achieve the best performance with a notable gain of 1.5%, 1.0%, 2.4% on the “MCC”, “Acc”, and F1 score respectively, compared to our proposed EKD. While \mathcal{L}_{inv} ensures that the synthesizable Fourier amplitudes are representative of what the free lunch model wants, capturing the frequency patterns in the frequency bands it was trained on, \mathcal{L}_{adv} is responsible for further exploring the latent space of the frozen model and making the frequency prompts more diverse than the ones previously distilled to the target model. (See Appendix A.1 for FPG output ablation)

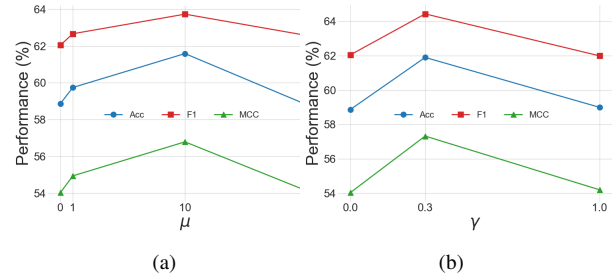


Figure 4: Sensitivity to μ and γ on the ISIC-LT Imbalance Ratio 1:500

Sensitivity of Balancing Regularization Batch normalization (BN) statistics are necessary for learning the Fourier prompts (FPG) in our proposed method. Similar to deep inversion and data-free knowledge distillation approaches [11], without BN, the FPG can be limited to balancing regularization. we perform ablation experiments on the balancing regularization weighting factor μ for the exploration phase proposed in Equation (6) over the extremest ISIC-LT setting (1:500). As shown in Figure 4 (a), we observe that a value of $\mu = 10$ increases the performance by 2.6%, 2.4%, and 2.5% on the “MCC”, “Acc”, and F1, respectively. Without using μ , the exploration phase is limited to the BN statistics without activation of the free-lunch model latent space, which can limit the representation transfer. A high value of μ , however, can negatively impact performance by encouraging the network to output a uniform distribution that is not discriminative nor informative.

Sensitivity of AKD Next, we investigate the effect of the adversarial factor γ proposed in Equation (9) on the performance of the extremest ISIC-LT setting (1:500). We found that a low value of γ (e.g., $\gamma = 0.3$) can enhance performance by making the Fourier prompts more diverse with iterative adversarial training, increasing the performance by 1.0% 2.0% on the F1-score and “MCC”, as shown in Figure 4 (b). On the other side, a high value of γ (e.g., $\gamma = 1$) results in a 2.0% drop in the F1-score. It is worth noting that, unlike other adversarial training approaches in domain adaptation, our focus is not on adversarial training but on synthesizing images based on the frozen pre-trained model by our proposed FPG. A lower value of γ ensures the diversity of generated prompts, whereas a higher value may result in FPG generating worst-case images with random amplitudes that the frozen pre-trained model cannot comprehend, leading to a decrease in overall performance.

EKD benefits LT even with smaller models The learning of the target model can be limited with an upper bound to the capacity of the free lunch model, f , and the MLP projector, and the information gained from f to the target task. However, we demonstrate in Table 6 that such limitations do not adversely affect the performance of the minority class

on ISIC-19 LT (“Tail”), with linear probed (LP) supervised ImageNet weights achieving 41.89% and EKD achieving 55.93% on the “Tail” accuracy. (See Appendix A.2 for “free lunch” model ablation)

Table 6: Effective Knowledge Distillation (EKD) with varying free lunch models. Results are averaged across 5 runs and across the three imbalance ratios (1:100, 1:200, 1:500) on the ISIC-LT dataset.

Method	Setting				Metric (%)	
	Target	Target Init	Free Lunch	Free Lunch Init	Tail	MCC
LP	None	None	RN-50	Sup-ImageNet	41.89	48.77
LP	None	None	RN-50	MoCov2	48.72	49.85
FT	None	None	RN-50	MoCov2	27.6	56.0
FT	None	None	RN-50	Sup-ImageNet	35.93	62.51
BSM	RN-18	None	None	None	46.6	59.32
EKD	RN-18	None	RN-50	Sup-ImageNet	51.47	61.13
BSM	RN-18	ImageNet	None	None	52.07	66.24
EKD	RN-18	ImageNet	RN-50	Sup ImageNet	55.93	68.09
EKD	RN-18	ImageNet	<u>RN-18</u>	Sup ImageNet	<u>55.87</u>	<u>67.18</u>

Our experiments presented in Table 6 demonstrate that our proposed EKD method can improve the performance of the target task even with smaller models. Specifically, we show that when given a target model g and its pre-trained version as the free lunch model f , EKD can benefit the tail classes using the frozen features from f despite f having the same capacity as g and being pre-trained on ImageNet. We observed a performance gain of 3.8% on tail class accuracy and 0.94% on “MCC” compared to the best-performing baseline initialized with ImageNet weights. It is worth mentioning that these results are averaged over 5 runs over the 3 class imbalance ratios (15 experiments). This phenomenon arises because fine-tuning can distort the pre-trained features, leading to a drop in generalization performance. However, the target model can further enhance its performance by using free discriminative distribution during training. While EKD can improve the performance of the target task even with smaller models, the best performance is achieved when using ResNet50 (RN50) as the free lunch model (f), with a performance gain of 1.85% and 1.81% on “MCC” compared to the baseline, BSM [29], when the target model is initialized randomly (None) or with ImageNet weights respectively. While most empirical evaluations ignore pre-trained initialization to provide fair and better convergence analysis, initialization unsurprisingly increases the averaged performance by 6.92% and 6.96% on “MCC” for the baseline and our proposed EKD, respectively. (See Appendix A.3 for the effectiveness of weight initialization)

5 Discussion

Rare disease classification is a crucial aspect of medical imaging, and leveraging publicly available pre-trained models can potentially improve the diagnosis and representations of these diseases. Existing work in this area of-

ten regularizes training on synthesizing worst-case scenarios and extracting the knowledge using closed-set datasets, without fully exploiting the generalization capabilities of widely known pre-trained models. Although some studies have explored effective prompting techniques for these models, their approaches are often limited to high-level features and prompt engineering without a deep understanding of how these “free lunch” encoders work, or how their representations can be further enhanced through a fundamental understanding of DNNs. In this work, we address this gap by investigating an intuitive phenomenon that has been widely neglected in the community: explicitly asking the pre-trained model what it wants, conditional on a cross-task medical input data, in order to gain insights into the learning dynamics of these models for effective representation learning. Through our method, we successfully demonstrate and leverage this phenomenon, shedding light on the inner workings of these models’ frequency patterns and their behavior toward representation learning. However, our proposed approach has certain limitations. One such limitation is the need for a better understanding of the learning dynamics of deep neural networks (DNNs) and the conditions required for capturing these frequency patterns. Recent studies have shown that DNNs rely on high-frequency patterns, which are typically ignored by radiologists for output representations [25]. Additionally, while skin lesions and gastrointestinal images can be considered out-of-distribution data for the free lunch model, there are extreme cases in medical imaging, such as X-rays and MRIs, which may require further exploration. Future research should aim to bridge the gap between natural image and medical imaging domains to enhance our understanding of the billions of parameters utilized in pre-trained models released every year. Additionally, further experiments on different tasks are needed to quantify the learning behavior of image encoders and understand what input these encoders want, as well as investigate the stability of the free lunch model over the FPG module. Theoretical proofs, rather than evaluations can also provide deeper insights into the dynamics of deep learning networks. Furthermore, this work may pave the way to understanding the counter-intuitive empirical phenomena of synthetic data in improving AI’s ability to predict test set error from the training set using GANs [38]. GANs may generate a synthetic dataset with frequency patterns that carry valuable information from the training set, while the model’s overfitting behavior to all the frequencies in the training set is a concern. Additionally, this work may offer insights into the factors contributing to the improved performance of AI segmentation with synthetic data [16]. The generators create enhanced datasets that focus on the highly informative patterns necessary for effective model training. Exploring the relationship between frequencies and the generation of synthetic data in medical imaging

opens up an intriguing avenue for future research.

6 Conclusion

In conclusion, our proposed FoPro-KD method provides an effective and efficient approach for compressing knowledge from publicly available pre-trained models to medical image classification tasks. We believe that future research should continue to explore the generalization capabilities of these largely available pre-trained models and develop methods to compress their knowledge for medical imaging tasks while preserving their generalization capabilities. Our method’s ability to utilize the pre-trained model’s knowledge to smaller target models for medical tasks can be particularly useful in clinical settings where affordable AI is needed. Overall, we believe that our FoPro-KD method represents a promising direction for addressing long-tailed classification problems and transfer learning in medical imaging.

A Appendix

A.1 FPG is conditional on both the input and the frozen free-lunch models

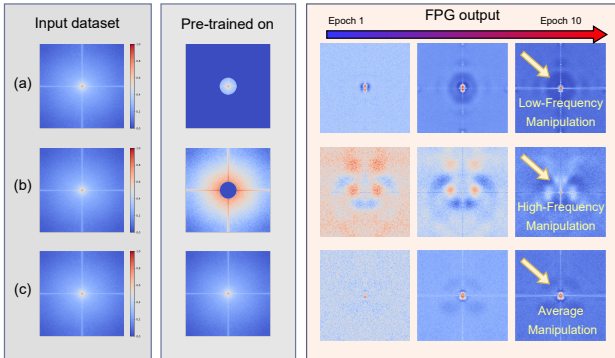


Figure 5: Average FPG generated prompts in three scenarios of pre-training f on different frequency components of the ISIC-LT dataset. (a) Pre-training f on only the low-frequency components. (b) Pre-training f on only the high-frequency components. (c) Pre-training f on all-frequency components.

In Figure 5, we demonstrate the behavior of our FPG with different settings. In (a), we trained the frozen pre-trained model, f , on only the low-frequency components of the ISIC-LT dataset. We observed that the FPG converged to a similar average amplitude as the input dataset but with different surpassing and amplification in the low-frequency parts that are conditional on f . (b) shows the FPG’s behavior when f was trained on only the high-frequency components of the ISIC-LT dataset. We found that the FPG attends

to the different frequencies in their higher frequencies that f has captured. Finally, in (c), we trained f on all frequency components of the input dataset. Interestingly, we found that the average amplitude generated by the FPG does not fully reduce to the amplitude of the source dataset, although it is conditional on the input dataset. This is because we do not have any prior knowledge of what frequency patterns in what frequency bands the pre-trained model extracts from the dataset in the pre-training stage. Nonetheless, FPG was able to amplify or suppress certain frequencies to provide understanding and interpretation of the behavior of pre-training models.

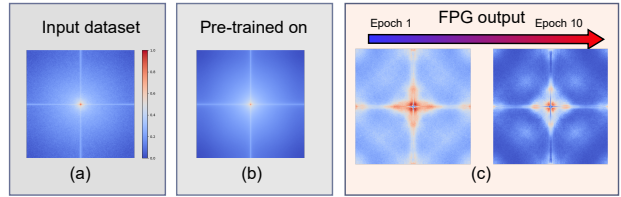


Figure 6: (a) Average ISIC-19 Fourier amplitude spectrum. (b) Average ImageNet Fourier amplitude spectrum. (c) FPG output in different epochs.

We show in Figure 6 when the frozen pre-trained model f is pre-trained on the ImageNet dataset with the average ImageNet Fourier spectrum. The generated output of our FPG is conditional on both the frequency patterns extracted by the pre-trained model f from the ImageNet Fourier spectrum and the frequency patterns of the target input dataset.

Our proposed Fourier Prompts Generator (FPG) is designed for understanding and interpreting the behavior of pre-trained models. Unlike prior methods that rely on adding noise to synthesize worst-case images, the FPG is conditional on both the input dataset and the frozen pre-trained model. We demonstrate in our analysis that the FPG can be used with only the L_{inv} and no adversarial training. Our method leverages the different frequency patterns captured in the pre-training stage of the network to amplify or suppress certain frequencies. By exploring these patterns with the FPG, we can gain insights into the specific input preferences of the pre-trained model that enable better representational transfer and interoperability. However, to enhance the generalizability and interpretability of our approach, further investigation is required into the distinct patterns of frequencies captured by the pre-trained model f , and their differences on more sophisticated models.

A.2 Free Lunch model Ablation

We present an ablation study of full fine-tuning and linear probing of the free lunch models pre-trained solely on ImageNet without any knowledge from our target task, used

with both the naive cross-entropy (CE) and the baseline, BSM [29].

As shown in Table 7, our experiments on linear probing models reveal that linear probing models initialized with MoCoV2 outperform models initialized with supervised ImageNet pre-training, with a performance gain of 2.26% and 6.83% on “Head” and “Tail” accuracy, respectively. This is because MoCoV2 learns competitive generalizable discriminative representations that benefit the tail classes in linear probing. Thus, our approach of leveraging models pre-trained solely on natural images without any prior knowledge from the target dataset proves to be effective.

On the other hand, full fine-tuning with the naive-cross entropy benefits the head classes more than linear probing with a gain of 25.18% on the “Head” but comes with a performance drop of 12.7% on the “Tail” in comparison with the best-performing linear probing. These models are computationally heavy for full-fine tuning and deployment, having almost two times the number of parameters as the target model (23 million vs 11 million parameters). Therefore, we propose EKD distilling and compressing such generalization capabilities to smaller models.

Table 7: Linear Probing (LP) and Fine-Tuning (FT) Accuracy of free lunch models with naive cross-entropy (CE), averaged over 5 runs across the three imbalance factors for the ISIC-LT dataset. The table includes the accuracy of the majority class (“Head”), the accuracy of the minority class (“Tail”), as well as the Matthew Correlation Coefficient (“MCC”), and the accuracy (“Acc”).

Setting		Metric (%)			
Method	Free Lunch	Head	Tail	MCC	Acc
LP	Sup-ImageNet	65.36	41.89	48.77	54.96
LP	MoCov2	67.62	48.72	49.85	55.99
FT	Random	88.23	22.88	49.46	54.63
FT	MoCov2	89.93	27.6	56.0	60.48
FT	Sup-ImageNet	92.8	35.93	62.51	66.34

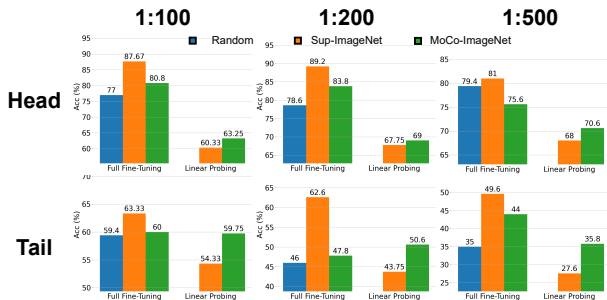


Figure 7: Bar plots illustrating the Linear Probing and Fine-Tuning Accuracy of free lunch models with baseline (BSM) [29] across three imbalance factors (1:100, 1:200, and 1:500) for the ISIC-LT dataset.

In Figure 7, we show the results of full fine-tuning and linear probing of the free lunch models utilized with the best-performing baseline, BSM [29]. We observed that the linear probing of the free lunch model (RN50) trained with contrastive learning (MoCov2) works better than the supervised version linear probed. The performance gain is 2.9%, 1.2%, and 2.6% on the head class and 5.4%, 6.9%, and 8.2% on the tail class for the three imbalance factors, respectively. This gain is attributed to the generalizable features from MoCo-v2 as reported previously. However, when fully fine-tuning the weights of the supervised ImageNet with the baseline [29], we observed compelling performance over both the head and tail classes compared to fully fine-tuning initialized with MoCov2. The performance gain is 6.8%, 5.4%, and 5.4% on the “Head” and 6.9%, 14.8%, and 5.6% on the “Tail” for the three imbalance factors, respectively. This gain can be attributed to the supervised ImageNet’s weights being already suited for supervision signals. These results are consistent for all three imbalance factors.

Our experiments have shown unsurprisingly that initialization methods play a crucial role in the performance of deep learning models on imbalanced datasets. While we show empirically that linear probing with contrastive learning approaches works best due to their superior generalization capabilities, we find that the supervised ImageNet initialization provided the best initialization performance for full fine-tuning of the free lunch model.

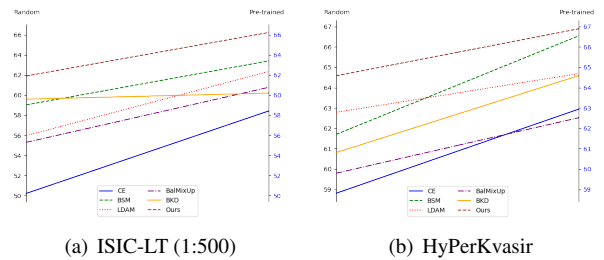


Figure 8: Initialization of target models with ImageNet pre-trained weights and random weights for all methods on ISIC-LT and HyperKvasir datasets. The left y-axis represents the performance of models initialized with random weights, while the right y-axis represents the performance of models initialized with ImageNet pre-trained weights.

A.3 Effectiveness of weight initialization

In Figure 8, we demonstrate the importance of weight initialization when dealing with long-tail learning. Recent works have mostly ignored such initialization steps in their empirical experiments to provide fair and better convergence analysis. We agree that pre-trained model weights are architecture-dependent and may not be available for

smaller models with the rising of large publicly available pre-trained models. However, if the smaller pre-trained model’s weights are available, it can offer a compelling starting point, increasing performance by 4.4% on “Acc” of ISIC-LT 1:500 with the baseline, BSM [29]. Moreover, initialization with pre-trained weights can further increase our FoPro-KD (“Ours”) performance by 5.0% on “Acc” on the ISIC-LT 1:500. Our method conserves the discriminative distribution capability while training through latent projections with EKD and input manipulation with FPG, which is vital for LT problems. We can also notice that BKD [37] is minimally affected on the ISIC 1:500 by pre-trained initialization (an increase of 0.61% on “Acc”).

On the HyperKvasir dataset, we observed that the performance of all methods improves when using the same optimization objective as in [12], namely stochastic gradient descent (SGD) with a learning rate of 0.01 and a cosine annealing scheduler.

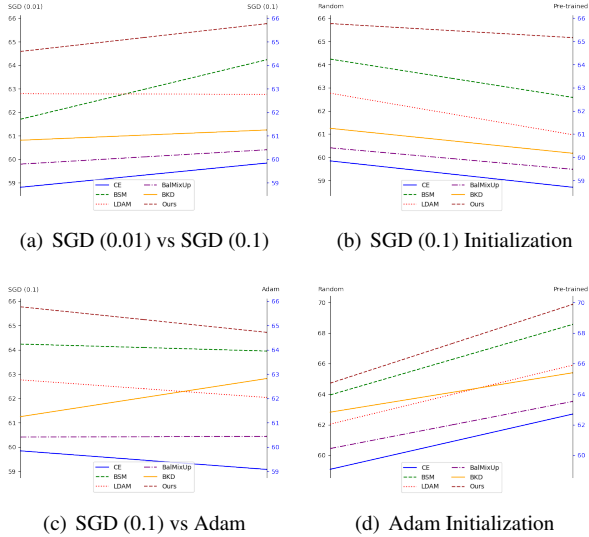


Figure 9: Comparison of different optimizers and different initialization on the HyperKvasir dataset. (a) and (c) depict experiments with different optimizers, while (b) and (d) represent experiments with different initialization.

In Figure 9, we present additional experiments conducted on the HyperKvasir dataset. In (a), we observe that SGD with a learning rate of 0.1 and cosine annealing scheduler was optimal for random initialization, outperforming the setting proposed in [12] and increasing the baseline performance [29] by 2.5% in terms of “B-Acc”. However, when using ImageNet initialization with SGD 0.1, we observe in (b) a negative impact on performance, possibly due to the high learning rate distorting the pre-trained features. Nevertheless, our proposed Effective Knowledge Distillation (EKD) approach demonstrates its benefits on both ran-

dom and pre-trained initialization in (b), with a minimal performance drop of 0.61% on “Ours” compared to a 1.65% drop on the best-performing baseline [29] in terms of “All”. Furthermore, we can notice in (b) that “Ours” and the BKD approach [37] are minimally affected by random and pre-trained model initialization. This can be attributed to the utilization of knowledge distillation, which helps maintain stability during training and prevents deviation in the target model’s performance. Additionally, our results showed that SGD with a learning rate of 0.1 converged to an optimal point more effectively than most methods when using Adam. However, when initializing with pre-trained weights and using Adam, we achieved a mean “B-Acc” of 69.9%. Overall, our proposed method consistently outperformed other approaches across different weight initialization and optimization strategies, demonstrating its effectiveness.

References

- [1] J. Bai, L. Yuan, S.-T. Xia, S. Yan, Z. Li, and W. Liu. Improving vision transformers by revisiting high-frequency components. In *ECCV*, 2022.
- [2] H. Borgli, V. L. Thambawita, P. H. Smedsrud, S. Hicks, D. Jha, S. L. Eskeland, K. R. Randel, K. Pogorelov, M. Lux, D. T. D. Nguyen, D. Johansen, C. Griwodz, H. K. Stensland, E. Garcia-Ceja, P. T. Schmidt, H. L. Hammer, M. Riegler, P. Halvorsen, and T. de Lange. Hyperkvasir, a comprehensive multi-class image and video dataset for gastrointestinal endoscopy. *Scientific Data*, 7, 2019.
- [3] K. Cao, C. Wei, A. Gaidon, N. Arechiga, and T. Ma. Learning imbalanced datasets with label-distribution-aware margin loss. In *Advances in Neural Information Processing Systems*, 2019.
- [4] C. Chen, Z. Li, C. Ouyang, M. Sinclair, W. Bai, and D. Rueckert. MaxStyle: Adversarial style composition for robust medical image segmentation. In *MICCAI*, 2022.
- [5] D. Chen, J.-P. Mei, H. Zhang, C. Wang, Y. Feng, and C. Chen. Knowledge distillation with the reused teacher classifier. In *Proceedings of the IEEE/CVF Conference on Computer Vision and Pattern Recognition*, pages 11933–11942, 2022.
- [6] M. Combalia, N. C. F. Codella, V. M. Rotemberg, B. Helba, V. Vilaplana, O. Reiter, A. C. Halpern, S. Puig, and J. Malvehy. Bcn20000: Dermoscopic lesions in the wild. *ArXiv*, abs/1908.02288, 2019.
- [7] Y. Cui, M. Jia, T.-Y. Lin, Y. Song, and S. Belongie. Class-balanced loss based on effective number of samples. In *Proceedings of the IEEE/CVF conference on computer vision and pattern recognition*, pages 9268–9277, 2019.
- [8] J. Deng, W. Dong, R. Socher, L.-J. Li, K. Li, and L. Fei-Fei. Imagenet: A large-scale hierarchical image database. In *2009 IEEE conference on computer vision and pattern recognition*, pages 248–255. Ieee, 2009.

- [9] X. Ding, Z. Liu, and X. Li. Free lunch for surgical video understanding by distilling self-supervisions. In L. Wang, Q. Dou, P. T. Fletcher, S. Speidel, and S. Li, editors, *MICCAI 2022*, volume 13437 of *Lecture Notes in Computer Science*, pages 365–375. Springer, 2022.
- [10] B. Dong, P. Zhou, S. Yan, and W. Zuo. LPT: Long-tailed prompt tuning for image classification. In *ICLR*, 2023.
- [11] G. Fang, J. Song, X. Wang, C. Shen, X. Wang, and M. Song. Contrastive model inversion for data-free knowledge distillation. *arXiv preprint arXiv:2105.08584*, 2021.
- [12] A. Galdran, G. Carneiro, and M. A. González Ballester. Balanced-mixup for highly imbalanced medical image classification. In M. de Bruijne, P. C. Cattin, S. Cotin, N. Padoy, S. Speidel, Y. Zheng, and C. Essert, editors, *Medical Image Computing and Computer Assisted Intervention – MICCAI 2021*, pages 323–333, Cham, 2021. Springer International Publishing.
- [13] I. J. Goodfellow, J. Pouget-Abadie, M. Mirza, B. Xu, D. Warde-Farley, S. Ozair, A. C. Courville, and Y. Bengio. Generative adversarial nets. In *NIPS*, 2014.
- [14] J.-B. Grill, F. Strub, F. Altché, C. Tallec, P. H. Richemond, E. Buchatskaya, C. Doersch, B. A. Pires, Z. D. Guo, M. G. Azar, B. Piot, K. Kavukcuoglu, R. Munos, and M. Valko. Bootstrap your own latent a new approach to self-supervised learning. In *NeurIPS*, NIPS’20, Red Hook, NY, USA, 2020. Curran Associates Inc.
- [15] K. He, H. Fan, Y. Wu, S. Xie, and R. B. Girshick. Momentum contrast for unsupervised visual representation learning. *CVPR*, pages 9726–9735, 2020.
- [16] Q. Hu, Y. Chen, J. Xiao, S. Sun, J. Chen, A. L. Yuille, and Z. Zhou. Label-free liver tumor segmentation. *ArXiv*, abs/2303.14869, 2023.
- [17] S. Hu, Z. Liao, and Y. Xia. Proslda: Prompt learning based source-free domain adaptation for medical image segmentation. *arXiv preprint arXiv:2211.11514*, 2022.
- [18] J. Huang, D. Guan, A. Xiao, and S. Lu. Rda: Robust domain adaptation via fourier adversarial attacking. *ICCV*, pages 8968–8979, 2021.
- [19] M. Jia, L. Tang, B.-C. Chen, C. Cardie, S. Belongie, B. Hariharan, and S.-N. Lim. Visual prompt tuning. In *European Conference on Computer Vision (ECCV)*, 2022.
- [20] L. Ju et al. Flexible sampling for long-tailed skin lesion classification. In *Medical Image Computing and Computer Assisted Intervention – MICCAI 2022*, pages 462–471, Cham, 2022. Springer Nature Switzerland.
- [21] B. Kang, S. Xie, M. Rohrbach, Z. Yan, A. Gordo, J. Feng, and Y. Kalantidis. Decoupling representation and classifier for long-tailed recognition. In *ICLR*, 2020.
- [22] M. Kim, D. Li, and T. Hospedales. Domain generalisation via domain adaptation: An adversarial fourier amplitude approach. In *ICLR*, 2023.
- [23] A. Kumar, A. Raghunathan, R. M. Jones, T. Ma, and P. Liang. Fine-tuning can distort pretrained features and underperform out-of-distribution. In *ICLR*, 2022.
- [24] I. Loshchilov and F. Hutter. SGDR: Stochastic gradient descent with warm restarts. In *ICLR*, 2017.
- [25] T. Makino, S. Jastrzebski, W. Oleszkiewicz, C. Chacko, R. Ehrenpreis, N. Samreen, C. Chhor, E. Kim, J. Lee, K. Pysarenko, B. Reig, H. Toth, D. Awal, L. Du, A. Kim, J. Park, D. K. Sodickson, L. Heacock, L. Moy, K. Cho, and K. J. Geras. Differences between human and machine perception in medical diagnosis. *Scientific Reports*, 12, 2020.
- [26] M. Mirza and S. Osindero. Conditional generative adversarial nets, 2014. cite arxiv:1411.1784.
- [27] A. Radford, J. W. Kim, C. Hallacy, A. Ramesh, G. Goh, S. Agarwal, G. Sastry, A. Askell, P. Mishkin, J. Clark, G. Krueger, and I. Sutskever. Learning transferable visual models from natural language supervision. In *ICML*, 2021.
- [28] A. Reinke et al. Metrics reloaded - a new recommendation framework for biomedical image analysis validation. In *Medical Imaging with Deep Learning*, 2022.
- [29] J. Ren, C. Yu, S. Sheng, X. Ma, H. Zhao, S. Yi, and H. Li. Balanced meta-softmax for long-tailed visual recognition. In *Proceedings of Neural Information Processing Systems (NeurIPS)*, Dec 2020.
- [30] K. Tang, M. Tao, J. Qi, Z. Liu, and H. Zhang. Invariant feature learning for generalized long-tailed classification. In *ECCV*, page 709–726, 2022.
- [31] P. Tschandl, C. Rosendahl, and H. Kittler. The ham10000 dataset, a large collection of multi-source dermatoscopic images of common pigmented skin lesions. *Scientific Data*, 5, 2018.
- [32] Y. Wang, J. Cheng, Y. Chen, S. Shao, L. Zhu, Z. Wu, T. Liu, and H. Zhu. Fvp: Fourier visual prompting for source-free unsupervised domain adaptation of medical image segmentation. *ArXiv*, abs/2304.13672, 2023.
- [33] C. Yang, X. Guo, Z. Chen, and Y. Yuan. Source free domain adaptation for medical image segmentation with fourier style mining. *Medical Image Analysis*, 79:102457, 2022.
- [34] J. Ye, Y. Ji, X. Wang, X. Gao, and M. Song. Data-free knowledge amalgamation via group-stack dual-gan. In *CVPR*, pages 12513–12522, 2020.
- [35] A. Yu, Y. Yang, and A. Townsend. Tuning frequency bias in neural network training with nonuniform data. In *ICLR*, 2023.
- [36] H. Zhang, M. Cisse, Y. N. Dauphin, and D. Lopez-Paz. mixup: Beyond empirical risk minimization. In *ICLR*, 2018.
- [37] S. Zhang, C. Chen, X. Hu, and S. Peng. Balanced knowledge distillation for long-tailed learning. *Neurocomputing*, 527:36–46, 2023.
- [38] Y. Zhang, A. Gupta, N. Saunshi, and S. Arora. On predicting generalization using GANs. In *International Conference on Learning Representations*, 2022.
- [39] G. Zhao, W. Yang, X. Ren, L. Li, and X. Sun. Well-classified examples are underestimated in classification with deep neural networks. In *AAAI Conference on Artificial Intelligence*, 2021.